

Towards Perfection: Building Inter-component Mutual Correction for Retinex-based Low-light Image Enhancement

Luyang Cao
Nanjing University
Nanjing, China
caoluyang@smail.nju.edu.cn

Han Xu
Southeast University
Nanjing, China
xu_han@seu.edu.cn

Jian Zhang
Nanjing University
Nanjing, China
zhang.jian@nju.edu.cn

Lei Qi
Southeast University
Nanjing, China
qilei@seu.edu.cn

Jiayi Ma
Wuhan University
Wuhan, China
jiayima@whu.edu.cn

Yinghuan Shi*
Nanjing University
Nanjing, China
syh@nju.edu.cn

Yang Gao
Nanjing University
Nanjing, China
gaoy@nju.edu.cn

Abstract

In low-light image enhancement, Retinex-based deep learning methods have garnered significant attention due to their exceptional interpretability. These methods decompose images into mutually independent illumination and reflectance components, allowing each component to be enhanced separately. In fact, achieving perfect decomposition of illumination and reflectance components proves to be quite challenging, with some residuals still existing after decomposition. In this paper, we formally name these residuals as inter-component residuals (ICR), which has been largely underestimated by previous methods. In our investigation, ICR not only affects the accuracy of the decomposition but also causes enhanced components to deviate from the ideal outcome, ultimately reducing the final synthesized image quality. To address this issue, we propose a novel Inter-correction Retinex model (IRetinex) to alleviate ICR during the decomposition and enhancement stage. In the decomposition stage, we leverage inter-component residual reduction module to reduce the feature similarity between illumination and reflectance components. In the enhancement stage, we utilize the feature similarity between the two components to detect and mitigate the impact of ICR within each enhancement unit. Extensive experiments on three low-light benchmark datasets demonstrated that by reducing ICR, our method outperforms state-of-the-art approaches both qualitatively and quantitatively. Our code is available at: <https://github.com/caoluyang0830/IRetinex.git>.

CCS Concepts

• Computing methodologies → Computer vision problems; Reconstruction.

*Corresponding Author.

Permission to make digital or hard copies of all or part of this work for personal or classroom use is granted without fee provided that copies are not made or distributed for profit or commercial advantage and that copies bear this notice and the full citation on the first page. Copyrights for components of this work owned by others than the author(s) must be honored. Abstracting with credit is permitted. To copy otherwise, or republish, to post on servers or to redistribute to lists, requires prior specific permission and/or a fee. Request permissions from permissions@acm.org.

MM '25, Dublin, Ireland

© 2025 Copyright held by the owner/author(s). Publication rights licensed to ACM.
ACM ISBN 979-8-4007-2035-2/2025/10
<https://doi.org/10.1145/3746027.3754973>

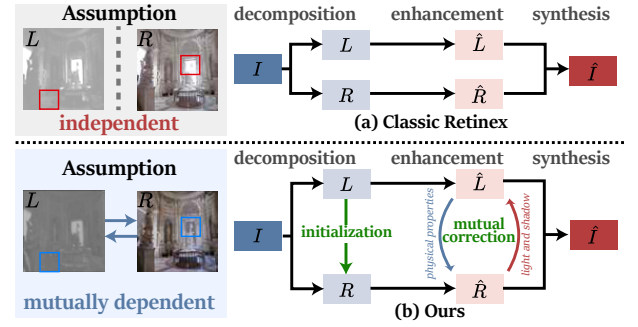


Figure 1: Comparison between the classic Retinex methods and our method. (a) The classic Retinex methods independently process illumination/reflectance, generating inter-component artifacts (red boxes). (b) Our method employs mutual correction during decomposition and enhancement, mitigating residuals and achieving satisfactory results.

Keywords

Retinex model, low-light image enhancement, inter-component residuals, mutual correction.

ACM Reference Format:

Luyang Cao, Han Xu, Jian Zhang, Lei Qi, Jiayi Ma, Yinghuan Shi, and Yang Gao. 2025. Towards Perfection: Building Inter-component Mutual Correction for Retinex-based Low-light Image Enhancement. In *Proceedings of the 33rd ACM International Conference on Multimedia (MM '25)*, October 27–31, 2025, Dublin, Ireland. ACM, New York, NY, USA, 16 pages. <https://doi.org/10.1145/3746027.3754973>

1 Introduction

In low-light condition, image quality degrades significantly, manifesting as low contrast, low visibility, dense noise, color distortions, etc [37]. In real applications, low-quality images not only impair human visual perception but also hinder computer vision systems in performing high-level image processing tasks, e.g., detection and recognition [4]. To address this challenge of multimodal perception optimization, low-light image enhancement (LLIE) has been proposed to correct color distortions and recover buried details in low-light conditions [18, 44, 48], thereby preserving the natural perception of human visual modality and simultaneously satisfying the demand of computer vision modality for feature representation.

With the development of deep learning, learning-based methods have become the mainstream approach for LLIE [1, 5, 54]. Among

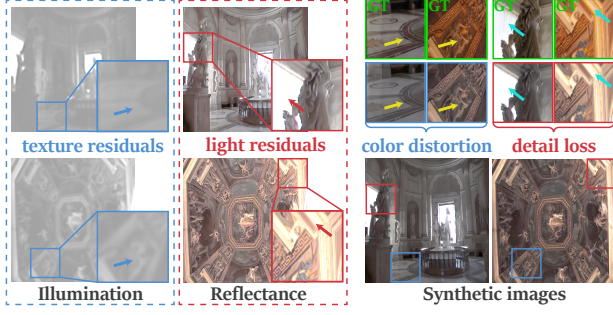


Figure 2: Method motivation. Imperfect decomposition leads to residuals remaining in the separated components. These residuals subsequently cause color distortion and detail loss in the synthesized images. GT: ground truth.

these approaches, the methods based on Retinex theory [1, 23, 42] have garnered significant attention due to its promising results. Mathematically, Retinex theory decomposes the image I into illumination L and reflectance R components:

$$I = L \odot R, \quad (1)$$

where \odot represents element-wise multiplication. As shown in Fig. 1, based on Retinex theory, low-light image enhancements contain three stages: 1) a *decomposition* stage to decouple the low-light image I into illumination component L (i.e., global light condition) and reflectance component R (i.e., physical properties including color and texture, etc), 2) an *enhancement* stage to adjust illumination \hat{L} and reflectance \hat{R} components separately, and 3) a *synthesis* stage to combine two components for the normal-light image \hat{I} . Taking advantage of the decomposition, Retinex-based methods effectively adapt to various lighting conditions and handle reflectance degradation, thereby achieving visually appealing results [5].

Despite their success, we found that existing methods are based on a fundamental yet idealized assumption: **illumination and reflectance are mutually independent** [23, 60]. Specifically, the reflectance component is required to be devoid of light or shadow (i.e., illumination information), while the illumination component should be free from physical properties (i.e., reflectance information). This assumption implies that, after decomposition, illumination and reflectance components should be perfectly separated, thus allowing their independent enhancement. However, in real cases, *Retinex decomposition is a highly ill-posed problem and there is no available ground truth for the illumination and reflectance components [5], which makes perfect decomposition challenging to achieve.*

To further illustrate this issue, we visualize the decomposition results of SOTA Retinex-based learning methods [47]. As shown in the left panel of Fig. 2, evidently, texture details (part of reflectance) bleed into the illumination component, and light and shadows (part of illumination) remain in the reflectance component (marked by the blue and red boxes in Fig. 2). During the enhancement stage, due to the existence of these residuals, the enhancement components inevitably deviate from the ideal outcome, ultimately degrading the quality of the final synthesized image, manifesting as color distortion and detail loss (shown in the right panel of Fig. 2). **In this paper, we investigate this issue that has been largely underestimated by previous methods, providing the first formal definition of these residuals as inter-component residuals (ICR).**

Based on above discussion, within the Retinex-based LLIE pipeline, reducing ICRs during the decomposition stage and mitigating their impact during the enhancement stage are crucial. Fortunately, as illustrated in the left panel of Fig. 2, we discovered that ICRs in the illumination component exhibit feature similarities to those in the corresponding reflectance component, and vice versa. This observation naturally prompts us to consider: **Could we leverage these feature similarities to identify and mitigate ICRs?**

Intuitively, during the decomposition stage, the low feature similarity between the illumination and reflectance components indicates that each component retains its inherent distinctive features, with no significant residuals. In the enhancement stage, the similar features actually reveal different component missed features. By supplementing these features into corresponding components, we could further drive the illumination and reflectance components closer to their ideal outcomes. Therefore, reducing feature similarity is beneficial to achieving perfect decomposition. Moreover, the similar features could facilitates mutual correction between the two components, thereby mitigating the ICR impact during the enhancement stage.

Based on the above analysis, we propose a novel inter-correction Retinex model (IRetinex) that systematically addresses ICR issues across both decomposition and enhancement stages. During the decomposition stage, we propose an innovative inter-component residual reduction module designed to minimize feature similarity between illumination and reflectance components, reducing initial decomposed ICR. During enhancement, we propose a novel module for residual mitigation and component enhancement. By leveraging feature similarity, this module identifies and mitigates ICRs across components and recovering buried details in low-light conditions. Additionally, we propose a Retinex-based multi-scale consistency loss that provides targeted supervision for the ICR identification process. Our contributions are summarized as follows:

- **An underestimated issue:** Imperfect decomposition results in ICR, causing deviations in illumination and reflectance components from their ideal states, ultimately degrading synthesized image quality.
- **An innovative solution:** ICR could be identified and mitigated by leveraging feature similarities between illumination and reflectance components.
- **A novel LLIE framework:** We propose an inter-correction Retinex framework that addresses ICR issue during both decomposition and enhancement stages.

Extensive experiments demonstrate that IRetinex outperforms state-of-the-art methods in both qualitative and quantitative evaluations. Moreover, it satisfies the requirements of computer vision applications for discriminative feature representation, achieving multimodal perception optimization.

2 Relate works

Traditional Retinex-based LLIE methods. Traditional Retinex-based LLIE methods are non-learning approaches that rely on ideal assumptions [9, 14–16, 31] or human prior knowledge [6, 10, 11, 21] to adjust image brightness and contrast. Some methods assume smooth light distribution across images and adjust estimated illumination to enhance brightness [6, 16], while others enhance local

contrast and color fidelity by assuming that physical properties remain invariant under different lighting conditions [14, 21]. However, their dependence on hand-crafted priors limits adaptability to real-world lighting variations.

Learning-based LLIE methods. Compared with traditional Retinex based methods, learning-based methods exhibit adaptability to diverse lighting scenes [13, 25, 43], which could be categorized into direct mapping methods and Retinex-based learning methods.

Direct mapping methods, aim to establish a image-to-image mapping from low-light to normal-light conditions. LL-Net makes the first attempt in this trail by developing a deep auto-encoder for contrast adjustment and noise removal [25]. Subsequently, a series of networks towards this goal are proposed [27, 32, 49]. Several works [33, 51, 63] employ wavelet transforms, gradient computations, and edge detectors for sharp and realistic structure enhancement. In [52, 62], color correction is performed through the utilization of color histograms and 3D lookup tables. To capture the statistical characteristics of visual signals, Li *et al.* formulate light enhancement as a task of image-specific curve estimation [20]. Recently, transformer-based methods with the guidance of signal-to-noise-ratio prior [50] and Fourier frequency information [36] also exhibit accurate and visually appealing results. Despite their success, image degradation is complex and uncertain (e.g., light enhancement, color distortion and structural blurring, etc.). Directly learning the image-to-image mapping to address these varied degradations is intricate and challenging [19].

Retinex-based learning methods. Different from direct mapping methods, Retinex-based learning methods [1, 56] have garnered significant attention due to their exceptional interpretability, as evidenced by Eq. (1). Fu *et al.* employ convolutional networks for reflectance texture recovery while employing transformers to model global illumination dependencies [5]. Yi *et al.* leverage diffusion models for light adjustment in illumination and detail enhancement in reflectance [56]. Since Zhang *et al.* demonstrate the efficacy of global illumination components in guiding image reconstruction [61], a series of illumination-guided low-light enhancement schemes are proposed [1, 39]. Ma *et al.* perform reflectance division utilizing illumination [29]. Cai *et al.* design an illumination-guided multi-head self-attention that utilizes illumination deep features to guide the computation of the mapping attention [1]. To achieve image-to-illumination mapping, Wang *et al.* introduce intermediate illumination with specialized loss functions to optimize the mapping process [39]. These approaches effectively advance the Retinex model performance in LLIE. However, we observe that existing methods typically assume that the illumination and reflectance is mutually independent. In real-world scenarios, the decomposition process inevitably suffers from the ICR issue, which causes the enhanced components to deviate from their ideal outcomes. This deviation ultimately degrades the quality of the final synthesized image. Therefore, it is very important to mitigate the impact of ICR to further boost the performance of Retinex models in LLIE.

3 Method

In this section, we mathematically prove the impact of ICR and introduce our overall framework: 1) inter-component residual reduction module, 2) residual mitigation with component enhancement module, and 3) Retinex-based multi-scale consistency loss.

3.1 Problem analysis of ICR

Based on the Retinex theory [17], a low light image I_l could be decomposed into illumination L_l and reflectance R_l . As mentioned in Sec. 1, achieving perfect decomposition is quite challenging. We assume that the residuals remaining in the illumination component is ϵ_R and remaining in the reflectance component is ϵ_L .

$$L_l = \hat{L}_l + \epsilon_R, \quad (2)$$

$$R_l = \hat{R}_l + \epsilon_L, \quad (3)$$

where \hat{L}_l and \hat{R}_l represent the ideal residual-free components. When enhancing these components utilizing functions $f_l(\cdot)$ and $f_r(\cdot)$, the residuals introduce estimation errors δ_L and δ_R , resulting in:

$$L_{en} = f_l(L_l) = \hat{L}_{en} + \delta_L, \quad (4)$$

$$R_{en} = f_r(R_l) = \hat{R}_{en} + \delta_R. \quad (5)$$

When synthesizing the enhanced image by combining these components, we get:

$$\begin{aligned} I_{en} &= (\hat{L}_{en} + \delta_L) \odot (\hat{R}_{en} + \delta_R) \\ &= \hat{L}_{en} + \underbrace{\hat{L}_{en} \odot \delta_R + \delta_L \odot \hat{R}_{en} + \delta_L \odot \delta_R}_{\text{estimation error}}, \end{aligned} \quad (6)$$

where \odot denotes element-wise multiplication, and \hat{L}_{en} represents the ideal enhancement outcome. If we express the deviation between the estimated and ideal image as E (where $I_{en} = \hat{L}_{en} \odot \hat{R}_{en} + E$), then $E = \hat{L}_{en} \odot \delta_R + \delta_L \odot \hat{R}_{en} + \delta_L \odot \delta_R$. Through algebraic manipulation, we can derive:

$$\delta_L = \frac{E - \delta_R \odot \hat{L}_{en}}{R_{en}}, \quad (7)$$

$$\delta_R = \frac{E - \delta_L \odot \hat{R}_{en}}{L_{en}}. \quad (8)$$

Assuming $E \sim \mathcal{N}(0, \sigma^2)$, $\delta_R \sim \mathcal{N}(0, \sigma^2)$, and $\delta_L \sim \mathcal{N}(0, \sigma^2)$, we observe that the distribution of δ_L is strongly related to R_{en} , and similarly, δ_R is strongly related to L_{en} . Therefore, **the estimation errors caused by ICR could be learned through a mutual correction way between illumination and reflectance components.** This crucial observation motivated the design of our IRetinex.

3.2 Our framework

As noted in Section 1, minimizing the initial ICR during decomposition and reducing its estimation errors in enhancement are critical. **In the decomposition stage**, we aim to preserve the unique features of illumination and reflectance components. It is widely recognized that the HSV color space separates illumination from color and saturation [3]. Therefore, the HSV color space provides a relatively pure illumination prior, which is beneficial for mitigating residuals in the illumination component. Based on this fact, we propose an inter-component residual reduction module (Sec. 3.3) to initialize the illumination and reflectance components with the assistance of HSV priors.

In the enhancement stage, driven by Eqs. (7) and (8), and our observation that ICRs visually resemble the features of their corresponding components, we could leverage feature similarity for component's mutual correction. Specifically, we propose a mutual residual estimation module (Sec. 3.4) to identify similar features

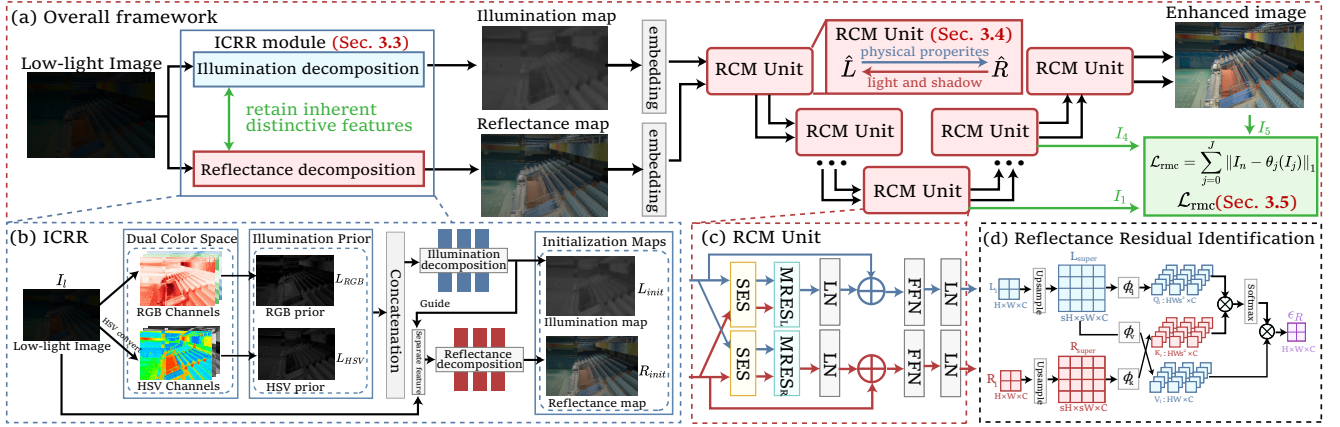


Figure 3: Overall architecture of IRetinex. The IRetinex consists of inter-component residual reduction module (ICRR), residual mitigation and component enhancement module (RCM) and Retinex-based multi-scale consistency loss (\mathcal{L}_{rmc}). In each RCM unite, dual-component mutually identify ICR and mitigate the accumulation of the estimation error.

(i.e., ICRs) between components, then integrate illumination and reflectance residuals into their corresponding components, thereby driving the components toward their ideal states. Furthermore, to recover detail losses caused by ICR, we design a super-resolution enhancement module (Sec. 3.4) to improve the sensitivity to texture detail. Additionally, we propose a Retinex-based multi-scale consistency loss (Sec. 3.5) to constrain ICR estimation.

3.3 Inter-component residual reduction module

As illustrated in Fig. 3 (b), our decomposition process for a low-light image I_l consists of two key stages: (1) illumination initialization and (2) reflectance initialization.

Illumination initialization. We estimate the illumination component through a hybrid approach combining RGB and HSV color spaces: 1) RGB-space initialization: Following conventional practice [1], we compute the mean across RGB channels to establish the initial RGB illumination prior $L_{rgb} = \frac{1}{3} \sum_{c \in \{r, g, b\}} I_{rgb}^{(c)}$. 2) HSV-space initialization: We convert the low-light input image I_l to HSV color space and extract the V channel as an auxiliary illumination prior $L_{hsv} = I_{hsv}^{(v)}$. For illumination map decomposition, we concatenate the input features I_l , L_{RGB} , and L_{HSV} along the channel dimension, applying convolution to adaptively separate light and shadows in low light image. Recognizing that large-scale convolutions are effective in modeling interactions between regions with varying illumination [1], we employ a large-scale convolution (i.e., kernel size 5×5) to capture light variation. The final illumination prior L_{init} is formulated as:

$$L_{init} = \psi_{1 \times 1}(\psi_{5 \times 5}(\psi_{1 \times 1}(\text{concat}(I_l, L_{RGB}, L_{HSV})))), \quad (9)$$

where $\psi_{1 \times 1}$ indicate convolution operation, $\text{concat}(\cdot)$ represent concatenation along the channel dimension.

Reflectance initialization. For reflectance component decomposition, according to Retinex theory [17], the reflectance component R_{init} could be obtained through $R_{init} = I_l / L_{init}$, where $/$ denotes the element-wise division. However, this simplistic and rudimentary decomposition typically results in color distortions [47]. To mitigate these distortions and preserve the inherent distinctive features of

reflectance components, we employ convolutional neural network to adaptively separate R_{init} from I_l :

$$R_{init} = \psi_{1 \times 1} \left(\psi_{5 \times 5} \left(\psi_{1 \times 1} \left(\text{concat} \left(I_l, \text{softmax} \left(\frac{I_l}{L_{init} + \epsilon} \right) \right) \right) \right) \right), \quad (10)$$

where $\text{softmax}(\cdot)$ denotes the softmax function, which normalizes the reflectance prior into a probability distribution, ϵ is a small constant to prevent division by zero. As illustrated in Fig. 4, ICRR reduces the inter-component similarity between decomposed illumination and reflectance images. Specifically, it minimizes texture residuals in the illumination component and eliminating light feature in the reflectance component.



Figure 4: ICRR reduces the feature similarity between illumination and reflectance, preserving the inherent discriminative features of each component.

3.4 Residual mitigation and component enhancement module

As illustrated in Fig. 3, our enhancement network adopts a multi-scale architecture based on the residual mitigation and component enhancement module (RCM), which consists of two key schemes: 1) a mutual residual estimation scheme (MRES) to simultaneously identify and mitigate ICRs across components, and 2) a super-resolution enhancement scheme (SES) that recovers buried details. Given the illumination and reflectance features (L_i and R_i) in layer i , the enhanced features by RCM (L_{i+1} and R_{i+1}) can be expressed as:

$$L_{i+1} = \text{FFN}(\text{MRES}(\text{SES}(R_i, L_i)) + L_i), \quad (11)$$

$$R_{i+1} = \text{FFN}(\text{MRES}(\text{SES}(L_i, R_i)) + R_i), \quad (12)$$

where Feed-Forward Network (FFN) consists of three convolutional layers with GELU activation. Layer Normalization is omitted for clarity. Below we detail MRES and SES.

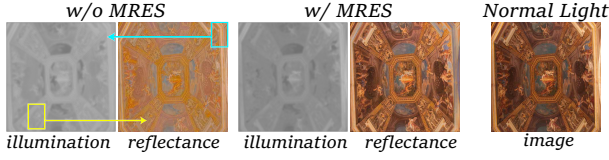


Figure 5: MRES transfers physical properties from illumination to reflectance and light features from reflectance to illumination.

Mutual residual estimation scheme. In MRES, we leverage inter-component feature similarity to capture ICR, then compensate the corresponding components with the identified residuals. Taking the illumination component as an example, first, we initialize Q_r , K_l with depth features from both component and initialize V_r from reflectance component:

$$Q_r = \phi_q(R_i), K_l = \phi_k(L_i), V_r = \phi_v(R_i), \quad (13)$$

where ϕ_q, ϕ_k, ϕ_v denote the parameter initialize layer of Q_r, K_l and V_r , respectively. Second, we compute the similarity matrix between reflectance and illumination features by utilizing Q_r and K_l . Subsequently, we leverage this matrix to extract similar features from the reflectance feature, thereby capturing the light and shadow residuals within the reflectance component. The estimated reflectance residual ϵ_L can be formulated as:

$$\epsilon_L = \text{softmax} \left(\frac{Q_r K_l^T}{d_i} \right) V_r, \quad (14)$$

where $d_i \in \mathbb{R}$ is a learnable parameter that adaptively scales the matrix multiplication. Similarly, we can obtain illumination residual ϵ_R in the same way:

$$\epsilon_R = \text{softmax} \left(\frac{Q_l K_r^T}{d_i} \right) V_l. \quad (15)$$

After reshaping, reflectance residual $\epsilon_R \in \mathbb{R}^{H \times W \times C}$ and illumination residual $\epsilon_L \in \mathbb{R}^{H \times W \times C}$ are added to original inputs L_i and R_i utilizing Eqs. (11) and (12). Fig. 5 visualizes the benefits of mutual residual estimation. Through MRES, we transfer light residuals from reflectance to illumination, and conversely, transfer texture residuals from illumination to reflectance, thereby driving both components closer to their ideal outcomes.

Super resolution enhancement SES aimed to recovers buried details caused by ICR. Specifically, for reflectance feature R_i and illumination feature L_i , we expand the feature resolution to initialize the high-resolution feature R_{super} and L_{super} , represented as:

$$R_{\text{super}} = \phi_r^s(R_i), L_{\text{super}} = \phi_l^s(L_i), \quad (16)$$

where $\phi_r^s(\cdot)$ and $\phi_l^s(\cdot)$ are the upsampling networks with deconvolution layer and convolution layers, and s is the scale factor. For capture illumination residual ϵ_R , we utilize upsampled feature R_{super} to initializes Q_r and K_l , the original resolution feature R_i initializes V_r , Eq. (13) can be rewritten as:

$$Q_r = \phi_q(R_{\text{super}}), K_l = \phi_k(L_{\text{super}}), V_r = \phi_v(R_i). \quad (17)$$

Leveraging the super-resolution features, we restore details compromised by ICRs. As illustrated in Fig. 6, SES refines edges, shapes, and structural details within deep features, which is beneficial in recovering textures obscured under low-light conditions. MRES

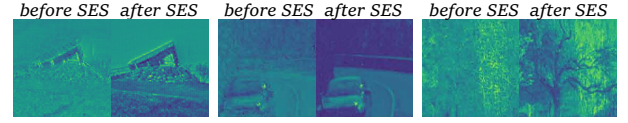


Figure 6: SES effectively enhance the finer details of deep features.

and SES constitute the RCM unit. A discussion of the complexity of RCM could be found in our supplementary material (Sec. B).

3.5 Retinex-based multi-scale consistency loss

Based on a multiscale network architecture, we could supervise ICR estimation at different scales. However, this supervision encounters two challenges: (1) Retinex decomposition is ill-posed [61], with no explicit ground truth for reflectance and illumination components; (2) Supervising multi-scale features requires downsampling the original ground truth, potentially losing detail. To avoid inappropriate supervision caused by ground truth decomposition, we reconstruct illumination and reflectance deep features into enhanced images:

$$I_j = \zeta_j^r(R_j) \odot \zeta_j^l(L_j), \quad (18)$$

where $j \in \{0, 1, 2, 3, 4\}$ denotes the network depth, $\zeta_j^r(\cdot)$ and $\zeta_j^l(\cdot)$ both consist of 3×3 convolutional layers for integrating high-dimensional deep features to synthesize the enhanced image $I_j \in \mathbb{R}^{\frac{H}{2^j} \times \frac{W}{2^j} \times 3}$.

To mitigate detail loss from ground truth downsampling, we upsample different enhanced images to match the ground truth resolution. We compute pixel-wise errors utilizing \mathcal{L}_1 loss:

$$\mathcal{L}_{\text{rmc}} = \sum_{j=0}^J \|I_n - \theta_j(I_j)\|_1, \quad (19)$$

where θ_j denotes the adaptive upsampling network for layer j , comprising convolutional and upsampling layers. \mathcal{L}_{rmc} enables ground truth to supervise multi-scale deep feature learning and optimize illumination and reflectance features jointly.

3.6 Summary

We now provide a summary, our IRetinex framework contains two stages: **In the decomposition stage**, ICRR (Section 3.3) first extracts the illumination component utilizing dual color space priors. This illumination component then facilitates reflectance extraction, reducing the initial ICR. **In the enhancement stage**, RCM (Section 3.4) enhances both illumination and reflectance components through a mutual correction way. Finally, \mathcal{L}_{rmc} (Section 3.5) supervises ICR estimation across multiple scales.

4 Experiment

4.1 Datasets and implementation details

Datasets. We evaluated our method on the LOL (v1 [46] and v2 [54]) datasets. LOL-v1 comprises 485 pairs of low-light/normal-light images for training and 15 pairs for testing. Each pair consists of a low-light input image and a corresponding well-exposed reference image. LOL-v2-real contains 689 pairs of low-light/normal-light images for training and 100 pairs for testing. Low-light images are mostly captured by adjusting exposure time and ISO while keeping other camera parameters fixed. LOL-v2-syn is generated by

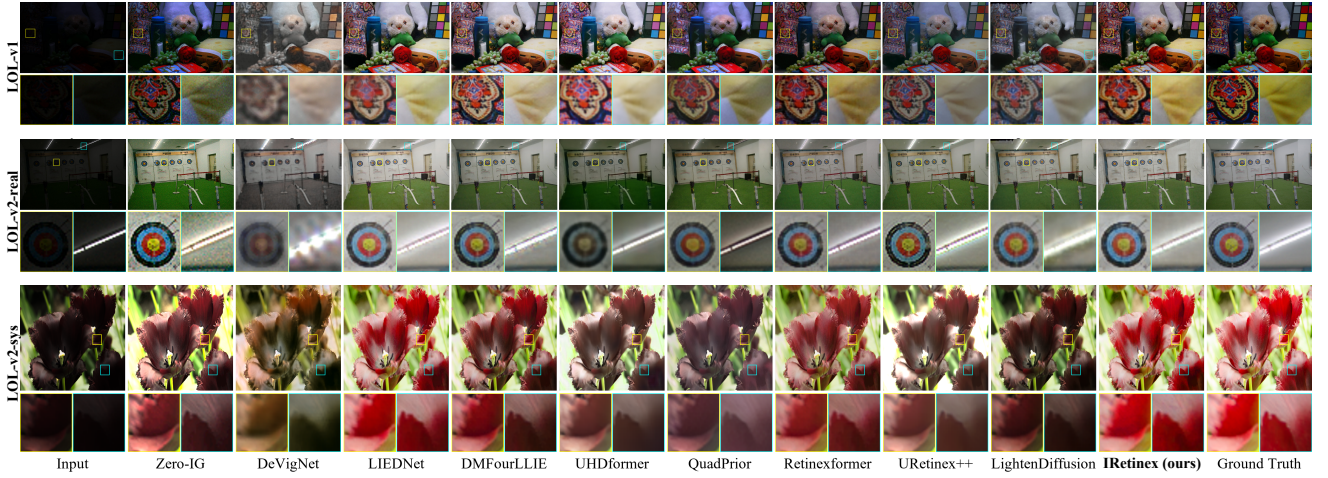


Figure 7: Visual comparison across LOL-v1, LOL-v2-real, and LOL-v2-syn datasets. Previous methods suffer from detail loss or color distortion, whereas our algorithm effectively recovers details and maintains color fidelity.

analyzing the illumination distribution in RAW format, the training and test sets are split proportionally into 900:100.

Implementation details. We implement IRetinex via PyTorch. The model is trained utilizing Adam optimizer ($\beta_1 = 0.9$, $\beta_2 = 0.999$) for 1.5×10^5 iterations. The learning rate is initially set to 2×10^{-4} and then steadily reduces to 1×10^{-6} by a cosine annealing scheme [26] during training. The batch size is 8. The training data is enhanced by random rotation and flipping. We utilize Peak Signal-to-Noise Ratio (PSNR), Structural Similarity (SSIM), and Learned Perceptual Image Patch Similarity (LPIPS) as evaluation metrics.

4.2 Low-light image enhancement

We evaluate our approach against 24 recent SOTA LLIE methods through qualitative and quantitative assessment.

Qualitative results. Figs. 7 present comparative results between IRetinex and existing methods on LOL-v1, LOL-v2-real, and LOL-v2-syn datasets. Enhanced images are evaluated based on color fidelity, texture preservation, and noise suppression. The first row demonstrate texture restoration capabilities. Under low-light conditions, the textures of the pillow and toy are degraded. Although comparison methods recovered partial details, Zero-IG exhibits significant noise compared to normal lighting images, DeVigNet shows blurred patterns on the pillow and fuzzy texture on the plush toy, while other methods suffer from varying degrees of texture loss and low color saturation. In contrast, IRetinex reconstructs texture details while maintaining color fidelity. The second row illustrates structural recovery from underexposed images. For an archery target, competing methods exhibit noise amplification (*i.e.*, Zero-IG, DMFourLLIE, URetinex++) and structural ambiguity (*i.e.*, DeVigNet, LIEDNet, UHDformer). In contrast, IRetinex reconstructs the target with minimal noise and enhanced texture detail. Moreover, when a lamp exists, simultaneously recovering both overexposed and underexposed regions is challenging. Existing methods exhibit limitations in color reproduction (*e.g.*, UHDformer, QuadPrior) and lamp structure reconstruction (*e.g.*, DeVigNet, DMFourLLIE, LightenDiffusion). Notably, IRetinex handles these exposure variations effectively and produces satisfactory enhancement results.

The last row presents a high-saturation image where accurate reproduction of vibrant red petal colors is challenging. Zero-IG, UHDformer, and QuadPrior exhibit color distortion. While LIEDNet and Retinexformer approximate the ground truth, they lack subtle tonal gradients within the petals. In comparison, IRetinex achieves accurate color saturation and preserving natural color transitions, maintaining fine chromatic variations.

Quantitative results. Tab. 1 presents the results on LOL-v1, LOL-v2-real, and LOL-v2-syn. The results were obtained from publications or by executing their public code. As shown in Tab. 1, IRetinex demonstrates strong performance across all three datasets. Compared to the SOTA algorithms on LOL-v1 and LOL-v2-syn, IRetinex improves PSNR by 1.94% and 3.23%, and SSIM by 1.13% and 1.64%, respectively. On LOL-v2-real, IRetinex achieve the best SSIM (0.8472 *v.s.* 0.8377). Additionally, the enhanced images from IRetinex exhibit better structure details and color fidelity than SNR-Net and URetinex++ (Fig. 7). Compared to other SOTA retinex-based deep learning methods (URetinex++ [47], LightenDiffusion [12], and Retinexformer [1]), our IRetinex achieves SSIM improvements of 0.0601, 0.0583 and 0.0133 across the three datasets. Different from these algorithms, IRetinex reduces the inherent inter-component residuals within the Retinex model, prompting the illumination and reflection components to approach their ideal outcomes. These improvements demonstrate that mitigating inter-component residuals benefits accurate enhancement results.

4.3 Ablation study and further analysis

Component ablation. We conducted an ablation study, with qualitative results in Fig. 8 and quantitative results in Tab. 2. Without ICRR, we observed PSNR decreases of 3.57dB, 3.58dB, and 2.86dB across datasets, with enhanced images exhibiting low color saturation and indistinct structural details. Removing MRES resulted in PSNR decreases of 2.41dB, 3.55dB, and 1.96dB, though these images maintained more realistic color and clearer structure than those without ICRR. This confirms that mutual assistance between illumination and reflectance components reduces estimation error in enhancement results. Without SES, enhanced images displayed

Table 1: Quantitative comparison on LOL-v1, LOL-v2-real, and LOL-v2-syn datasets. The highest result is bolded, while the second highest result is underlined.

Methods	Venue	LOL-v1			LOL-v2-real			LOL-v2-syn		
		PSNR↑	SSIM↑	LPIPS↓	PSNR↑	SSIM↑	LPIPS↓	PSNR↑	SSIM↑	LPIPS↓
RetinexNet [46]	BMVC'18	17.54	0.7136	0.3846	17.65	0.6127	0.4459	17.30	0.7632	0.3833
KinD [61]	ACM MM'19	19.66	0.7936	0.1577	15.68	0.7142	0.3964	16.80	0.6930	0.3609
Zero-DCE [7]	CVPR'20	15.04	0.4514	0.4032	16.94	0.5268	0.4488	16.25	0.6405	0.2139
MIRNet [58]	ECCV'20	24.13	0.8279	0.1280	20.44	0.7487	0.3325	23.41	0.9093	0.0946
DRBN [53]	CVPR'20	21.30	0.7889	0.2179	20.77	0.7569	0.2715	19.94	0.8142	0.2136
EnGAN [13]	TIP'21	17.48	0.6583	0.3142	18.84	0.6286	0.3061	16.57	0.7923	0.2212
SGM [55]	TIP'21	17.81	0.7648	0.2185	20.06	0.8191	0.1627	22.05	0.9031	0.0902
RUAS [23]	CVPR'21	14.63	0.5726	0.2846	17.97	0.6459	0.3289	16.94	0.6483	0.2215
Restormer [57]	CVPR'22	21.71	0.7500	0.2179	22.43	0.7594	0.2684	20.70	0.8025	0.1954
Uformer [45]	CVPR'22	19.20	0.7876	0.2821	18.60	0.6357	0.4276	18.21	0.7522	0.2129
SNR-Net [50]	CVPR'22	24.61	<u>0.8417</u>	0.1501	21.48	0.8314	0.1590	24.13	0.9303	0.0609
SCI [30]	CVPR'22	17.35	0.6821	0.2077	16.69	0.5940	0.3480	17.50	0.7163	0.2171
LLFormer [40]	AAAI'23	23.64	0.8092	0.1641	20.74	0.8175	0.1622	23.16	0.9099	0.0925
FourLLIE [36]	ACM MM'23	20.58	0.6929	0.1646	22.34	0.8220	0.1135	24.64	0.9175	0.0690
Bread [8]	IJCV'23	18.07	0.7124	0.2436	18.94	0.7659	0.2598	17.06	0.8226	0.1918
Retinexformer [1]	CVPR'23	25.15	0.8402	0.1272	22.79	<u>0.8377</u>	0.1691	25.67	0.9380	0.0639
DMFourLLIE [59]	ACM MM'24	22.43	0.8012	0.1241	18.86	0.8214	<u>0.1216</u>	24.89	0.9350	0.0546
UHDFormer [35]	AAAI'24	22.88	0.8350	0.1366	18.57	0.6457	0.4167	17.46	0.7468	0.2692
QuadPrior [41]	CVPR'24	18.33	0.7675	0.2048	20.59	0.7600	0.2003	17.10	0.7457	0.3167
DeVigNet [28]	AAAI'24	20.71	0.7123	0.2079	19.81	0.5607	0.4612	18.67	0.6802	0.3056
Zero-IG [34]	CVPR'24	22.71	0.8089	0.1949	18.13	0.6932	0.2448	17.43	0.7307	0.2121
LightenDiffusion [12]	ECCV'24	19.12	0.7486	0.1954	21.71	0.7889	0.1871	19.94	0.8263	0.1700
LIEDNet [22]	TCSVT'25	24.79	0.8254	0.1234	20.29	0.8181	0.1669	<u>26.00</u>	<u>0.9431</u>	<u>0.0496</u>
URetinex++ [47]	TPAMI'25	23.83	0.8186	<u>0.1154</u>	23.92	0.7981	0.1872	18.99	0.7443	0.2101
IRetinex (ours)	-	25.64	0.8787	0.1107	<u>23.56</u>	0.8472	0.1675	26.84	0.9513	0.0488

Table 2: Results of the ablation study.

Datasets	Methods	PSNR↑	SSIM↑	LPIPS↓
LOL-v1	Ours w/o ICRR	22.07	0.8509	0.1289
	Ours w/o MRES	23.23	0.8534	0.1233
	Ours w/o SES	24.85	0.8657	0.1175
	Ours w/o \mathcal{L}_{rmc}	25.09	0.8702	0.1132
	IRetinex (ours)	25.64	0.8787	0.1107
LOL-v2-real	Ours w/o ICRR	19.98	0.8265	0.1896
	Ours w/o MRES	20.01	0.8309	0.1803
	Ours w/o SES	21.56	0.8358	0.1782
	Ours w/o \mathcal{L}_{rmc}	22.98	0.8432	0.1763
	IRetinex (ours)	23.56	0.8472	0.1675
LOL-v2-syn	Ours w/o ICRR	23.98	0.9102	0.0914
	Ours w/o MRES	24.88	0.9217	0.0698
	Ours w/o SES	25.64	0.9109	0.0512
	Ours w/o \mathcal{L}_{rmc}	26.01	0.9352	0.0490
	IRetinex (ours)	26.84	0.9513	0.0488

Table 3: Ablation studies of the loss function terms.

Datasets	Methods	PSNR↑	SSIM↑	LPIPS↓
LOL-v1	Ours w/o RBS	25.12	0.8653	0.1203
	Ours w/o ISR	25.47	0.8698	0.1172
	IRetinex (ours)	25.64	0.8787	0.1107
LOL-v2-real	Ours w/o RBS	22.67	0.8404	0.1788
	Ours w/o ISR	23.01	0.8418	0.1704
	IRetinex (ours)	23.56	0.8472	0.1675
LOL-v2-syn	Ours w/o RBS	25.67	0.9405	0.0514
	Ours w/o ISR	26.36	0.9499	0.0503
	IRetinex (ours)	26.84	0.9513	0.0488

**Figure 8: Visual comparisons for ablation study on LOL-v2-syn dataset. Ground truth shown in yellow rectangles.**

blurred structures and indistinct boundaries, with SSIM decreases of 0.0130, 0.0114, and 0.0404 across datasets. The absence of \mathcal{L}_{rmc} supervision for deep features led to PSNR decreases of 0.55dB, 0.58dB, and 0.83dB, resulting in reduced brightness and blurred structures. Our complete IRetinex achieved the highest PSNR and SSIM scores, demonstrating the contribution of each component to low-light image enhancement.

Effectiveness of Retinex-based multi-scale consistency loss.

We conducted experiments by separately removing the image super-resolution (ISR) and Retinex-based supervision (RBS) components, with quantitative results presented in Tab. 3. As shown in the first row, removing RBS led to performance degradation due to the inherent ill-posed nature of Retinex decomposition. The second row reveals the limitations of utilizing low-resolution images for supervision, where performance decreased across all three datasets because of detail loss in the downsampled ground truth.

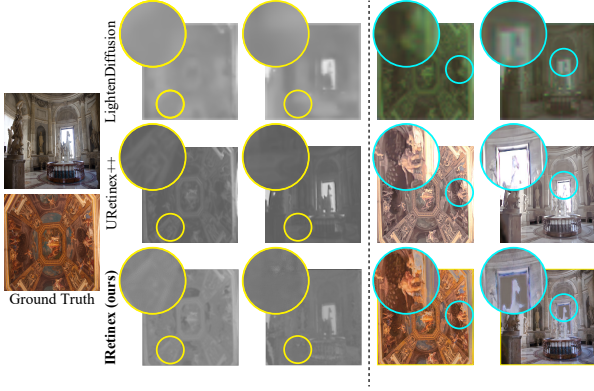


Figure 9: Decomposition results of LLIE methods based on Retinex model on the LOL-v2-syn dataset. All illumination and reflectance components are extracted based on their original implementations.

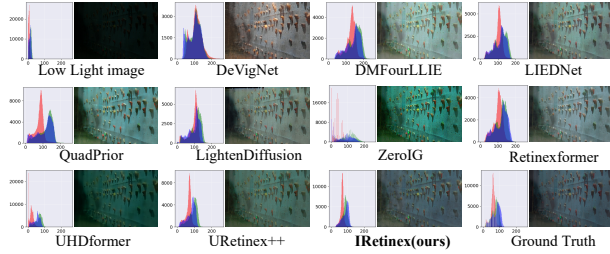


Figure 10: RGB histogram comparison of IRetinex and other LLIE methods on the LOL-v2-real dataset. Red, green, and blue represent R, G, and B color distributions respectively. The x-axis denotes pixel values [0-255], while the y-axis indicates pixel count.

Effectiveness and benefits of ICR mitigation. In ideal Retinex decomposition, illumination components exhibit uniform distribution across identical materials, and reflectance components accurately represent physical properties without lighting effects. Our experimental results demonstrate IRetinex’s performance in mitigating ICR compared to recent Retinex-based methods. As shown in Fig. 9, URetinex++ retain textures in illumination components and display lighting residuals in reflectance components. Illumination components of LightenDiffusion are excessively smooth, with different materials exhibiting identical lighting, and the components miss textures and exhibit severe color deviation. In contrast, our method separates these components effectively. It produces illumination components with accurate light distributions and reflectance components that faithfully preserve physical details without color distortion or texture blurring. The benefits of this ICR mitigation appear in both color and structural distributions of enhanced images. RGB histograms (Fig. 10) show that IRetinex aligns with ground truth, effectively correcting the limited dynamic range characteristic of low-light images. Similarly, structural error maps (Fig. 11) reveal that competing methods introduce artifacts or suffer from detail loss, whereas IRetinex minimizes structural errors and preserves fine details. These results confirm that effective ICR mitigation leads to enhanced low-light images that match normal-light references both visually and in quantitative measures. Our supplementary

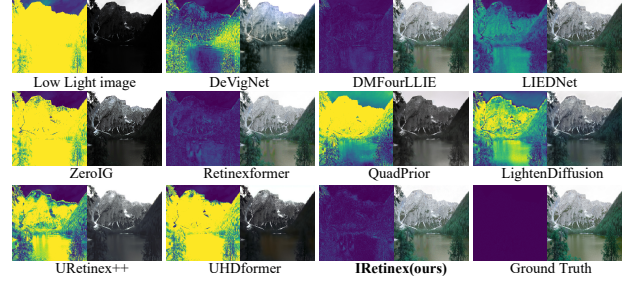


Figure 11: Texture error map comparison between IRetinex and other LLIE methods on the LOL-v2-syn dataset. Color proximity to yellow indicates larger discrepancies, while proximity to blue denotes smaller differences.

materials (Sec. F, Sec. G) provide extended comparative results. **Enhancement of high-level vision tasks.** To evaluate performance on high-level vision tasks, we applied enhanced images to challenging low-light object detection scenarios. Specifically, we trained the YOLOv7 detector [38] on the ExDark dataset [24] using images enhanced by different LLIE methods. As illustrated in Fig. 12, key object features are severely degraded under low-light conditions, bringing substantial challenges for object detection. While existing LLIE methods successfully recover obscured subjects and improve detection accuracy, our IRetinex-enhanced images exhibit sharper object boundaries and superior color fidelity, leading to further improvements in detection performance (e.g., increasing cat recognition precision from 0.39 to 0.91). These results demonstrate our method’s effectiveness in enhancing high-level vision tasks under extreme low-light conditions. In summary, the IRetinex-enhanced images maintain natural visual perception compatible with human vision while simultaneously satisfying the requirements of computer vision systems for robust feature representation. Additional qualitative visualizations and quantitative analyses are provided in the supplementary materials (Sec. E).

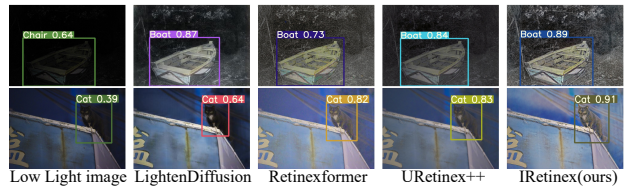


Figure 12: Object detection performance in low-light and enhanced images on the ExDark dataset.

5 Conclusion

This work addresses a critical but overlooked challenge issue termed the inter-component residual (ICR), which arises from imperfect decomposition and degrades illumination and reflectance estimation. We discover that ICR could be mitigated by exploiting feature similarities between the two components and propose IRetinex, a novel inter-correction framework that mitigates ICR at both decomposition and enhancement stages. Extensive experiments demonstrate that IRetinex outperforms SOTA algorithms across three benchmark datasets. Crucially, our framework jointly optimizes for human vision and computer vision modalities, highlighting the importance of modeling intrinsic decomposition errors and offering a principled approach for advancing Retinex-based LLIE.

Acknowledgments

This work is supported by NSFC Project (62222604, 62206052), China Postdoctoral Science Foundation (2024M750424), Fundamental Research Funds for the Central Universities (020214380120, 020214380128), State Key Laboratory Fund (ZZKT2024A14, ZZKT2025B05), Postdoctoral Fellowship Program of CPSF (GZC20240252), Jiangsu Funding Program for Excellent Postdoctoral Talent (2024ZB242) and Jiangsu Science and Technology Major Project (BG2024031).

References

- [1] Yuanhao Cai, Hao Bian, Jing Lin, Haoqian Wang, Radu Timofte, and Yulun Zhang. 2023. Retinexformer: One-stage Retinex-based Transformer for Low-light Image Enhancement. In *ICCV*. 12504–12513.
- [2] Chen Chen, Qifeng Chen, Minh N. Do, and Vladlen Koltun. 2019. Seeing Motion in the Dark. In *ICCV*.
- [3] Zhi Dou, Ning Wang, Baopu Li, Zhihui Wang, Haojie Li, and Bin Liu. 2021. Dual Color Space Guided Sketch Colorization. *IEEE Trans. Image Process.* 30 (2021), 7292–7304. doi:10.1109/TIP.2021.3104190
- [4] Hansen Feng, Lizhi Wang, Yuzhi Wang, Haoqiang Fan, and Hua Huang. 2024. Learnability Enhancement for Low-Light Raw Image Denoising: A Data Perspective. *IEEE Trans. Pattern Anal. Mach. Intell.* 46, 1 (Jan. 2024), 370–387. doi:10.1109/TPAMI.2023.3301502
- [5] Huiyuan Fu, Wenkai Zheng, Xiangyu Meng, Xin Wang, Chuanming Wang, and Huadong Ma. 2023. You Do Not Need Additional Priors or Regularizers in Retinex-Based Low-Light Image Enhancement. In *CVPR*. 18125–18134.
- [6] Xueyang Fu, Delu Zeng, Yue Huang, Xiao-Ping Zhang, and Xinghao Ding. 2016. A Weighted Variational Model for Simultaneous Reflectance and Illumination Estimation. In *Proceedings of the IEEE Conference on Computer Vision and Pattern Recognition (CVPR)*.
- [7] Chunle Guo, Chongyi Li, Jichang Guo, Chen Change Loy, Junhui Hou, Sam Kwong, and Runmin Cong. 2020. Zero-Reference Deep Curve Estimation for Low-Light Image Enhancement. In *CVPR*. 1777–1786. doi:10.1109/CVPR42600.2020.00185
- [8] Xiaojie Guo and Qiming Hu. 2023. Low-Light Image Enhancement via Breaking Down the Darkness. *Int. J. Comput. Vis* 131, 1 (2023), 48–66. doi:10.1007/s11263-022-01667-9
- [9] Xiaojie Guo, Yu Li, and Haibin Ling. 2017. LIME: Low-Light Image Enhancement via Illumination Map Estimation. *IEEE Transactions on Image Processing* 26, 2 (2017), 982–993. doi:10.1109/TIP.2016.2639450
- [10] Xiaojie Guo, Yu Li, and Haibin Ling. 2017. LIME: Low-Light Image Enhancement via Illumination Map Estimation. *IEEE Trans. Image Process.* 26, 2 (Feb. 2017), 982–993. doi:10.1109/TIP.2016.2639450
- [11] Shijie Hao, Xu Han, Yanrong Guo, Xin Xu, and Meng Wang. 2020. Low-Light Image Enhancement With Semi-Decoupled Decomposition. *IEEE Transactions on Multimedia* 22, 12 (2020), 3025–3038. doi:10.1109/TMM.2020.2969790
- [12] Hai Jiang, Ao Luo, Xiaohong Liu, Songchen Han, and Shuaicheng Liu. 2024. LightDiffusion: Unsupervised Low-Light Image Enhancement with Latent-Retinex Diffusion Models. In *European Conference on Computer Vision*.
- [13] Yifan Jiang, Xinyu Gong, Ding Liu, Yu Cheng, Chen Fang, Xiaohui Shen, Jianchao Yang, Pan Zhou, and Zhangyang Wang. 2021. EnlightenGAN: Deep Light Enhancement Without Paired Supervision. *IEEE Trans. Image Process.* 30 (2021), 2340–2349. doi:10.1109/TIP.2021.3051462
- [14] D.J. Jobson, Z. Rahman, and G.A. Woodell. 1997. A multiscale retinex for bridging the gap between color images and the human observation of scenes. *IEEE Transactions on Image Processing* 6, 7 (1997), 965–976. doi:10.1109/83.597272
- [15] D.J. Jobson, Z. Rahman, and G.A. Woodell. 1997. Properties and performance of a center/surround retinex. *IEEE Transactions on Image Processing* 6, 3 (1997), 451–462. doi:10.1109/83.557356
- [16] Ron Kimmel, Michael Elad, Doron Shaked, Renato Keshet, and Irwin Sobel. 2003. A Variational Framework for Retinex. *International Journal of Computer Vision* 52, 1 (April 2003), 7–23. doi:10.1023/A:1022314423998
- [17] Edwin H. Land. 1977. The Retinex Theory of Color Vision. *Scientific American* 237, 6 (1977), 108–129. <http://www.jstor.org/stable/24953876>
- [18] Chongyi Li, Chunle Guo, Linghao Han, Jun Jiang, Ming-Ming Cheng, Jinwei Gu, and Chen Change Loy. 2021. Low-Light Image and Video Enhancement Using Deep Learning: A Survey. *IEEE Trans. Pattern Anal. Mach. Intell.* 44, 12 (2021), 9396–9416.
- [19] Chongyi Li, Chunle Guo, Linghao Han, Jun Jiang, Ming-Ming Cheng, Jinwei Gu, and Chen Change Loy. 2021. Low-Light Image and Video Enhancement Using Deep Learning: A Survey. *IEEE Trans. Pattern Anal. Mach. Intell.* 44, 12 (2021), 9396–9416.
- [20] Chongyi Li, Chunle Guo, and Chen Change Loy. 2022. Learning to Enhance Low-Light Image via Zero-Reference Deep Curve Estimation. *IEEE Trans. Pattern Anal. Mach. Intell.* 44, 8 (Aug. 2022), 4225–4238. doi:10.1109/TPAMI.2021.3063604
- [21] Mading Li, Jiaying Liu, Wenhan Yang, Xiaoyan Sun, and Zongming Guo. 2018. Structure-Revealing Low-Light Image Enhancement Via Robust Retinex Model. *IEEE Transactions on Image Processing* 27, 6 (2018), 2828–2841. doi:10.1109/TIP.2018.2810539
- [22] Mingyu Liu, Yuning Cui, Wenqi Ren, Juxiang Zhou, and Alois C. Knoll. 2025. LLEDNet: A Lightweight Network for Low-light Enhancement and Deblurring. *IEEE Transactions on Circuits and Systems for Video Technology* (2025), 1–1. doi:10.1109/TCSVT.2025.3541429
- [23] Risheng Liu, Long Ma, Jiaao Zhang, Xin Fan, and Zhongxuan Luo. 2021. Retinex-Inspired Unrolling with Cooperative Prior Architecture Search for Low-light Image Enhancement. In *CVPR*. 10556–10565. doi:10.1109/CVPR46437.2021.01042
- [24] Yuen Peng Loh and Chee Seng Chan. 2019. Getting to Know Low-Light Images with the Exclusively Dark Dataset. *Comput. Vis. Image. Und.* 178 (2019), 30–42. doi:10.1016/j.cviu.2018.10.010
- [25] Kin Gwn Lore, Adedotun Akintayo, and Soumik Sarkar. 2017. LLNet: A Deep Autoencoder Approach to Natural Low-Light Image Enhancement. *Pattern. Recogn.* 61 (2017), 650–662. doi:10.1016/j.patcog.2016.06.008
- [26] Ilya Loshchilov and Frank Hutter. 2017. SGDR: Stochastic Gradient Descent with Warm Restarts. In *ICLR*.
- [27] Kun Lu and Lihong Zhang. 2020. TBEFN: A Two-Branch Exposure-Fusion Network for Low-Light Image Enhancement. *IEEE Transactions on Multimedia* 23 (2020), 4093–4105.
- [28] Shenghong Luo, Xuhang Chen, Weiwen Chen, Zinuo Li, Shuqiang Wang, and Chi-Man Pun. 2024. Devignet: High-Resolution Vignetting Removal via a Dual Aggregated Fusion Transformer with Adaptive Channel Expansion. In *AAAI*, Vol. 38. 4000–4008.
- [29] Long Ma, Dian Jin, Nan An, Jinyuan Liu, Xin Fan, Zhongxuan Luo, and Risheng Liu. 2023. Bilevel Fast Scene Adaptation for Low-Light Image Enhancement. *Int. J. Comput. Vis* (Oct. 2023). doi:10.1007/s11263-023-01900-z
- [30] Long Ma, Tengyu Ma, Risheng Liu, Xin Fan, and Zhongxuan Luo. 2022. Toward Fast, Flexible, and Robust Low-Light Image Enhancement. In *CVPR*. 5627–5636. doi:10.1109/CVPR52688.2022.00555
- [31] Michael K. Ng and Wei Wang. 2011. A Total Variation Model for Retinex. *SIAM Journal on Imaging Sciences* 4, 1 (2011), 345–365. doi:10.1137/100806588
- [32] Wenqi Ren, Sifei Liu, Lin Ma, Qianqian Xu, Xiangyu Xu, Xiaochun Cao, Junping Du, and Ming-Hsuan Yang. 2019. Low-Light Image Enhancement via a Deep Hybrid Network. *IEEE Trans. Image Process.* 28, 9 (2019), 4364–4375.
- [33] Wenqi Ren, Sifei Liu, Lin Ma, Qianqian Xu, Xiangyu Xu, Xiaochun Cao, Junping Du, and Ming-Hsuan Yang. 2019. Low-Light Image Enhancement via a Deep Hybrid Network. *IEEE Trans. Image Process.* 28, 9 (Sept. 2019), 4364–4375. doi:10.1109/TIP.2019.2910412
- [34] Yiqi Shi, Duo Liu, Liguo Zhang, Ye Tian, Xuezhi Xia, and Xiaojing Fu. 2024. ZERO-IG: Zero-Shot Illumination-Guided Joint Denoising and Adaptive Enhancement for Low-Light Images. In *CVPR*. 3015–3024.
- [35] Cong Wang, Jinshan Pan, Wei Wang, Gang Fu, Siyuan Liang, Mengzhu Wang, Xiao-Ming Wu, and Jun Liu. 2024. Correlation Matching Transformation Transformers for UHD Image Restoration. *Proceedings of the AAAI Conference on Artificial Intelligence* 38, 6 (Mar. 2024), 5336–5344. doi:10.1609/aaai.v38i6.28341
- [36] Chenxi Wang, Hongjun Wu, and Zhi Jin. 2023. FourLLIE: Boosting Low-Light Image Enhancement by Fourier Frequency Information. In *ACM MM*. 7459–7469.
- [37] Chao Wang, Yang Zhou, Liangtian He, Fenglai Lin, Hongming Chen, and Liang-Jian Deng. 2024. Illumination Distribution Prior for Low-light Image Enhancement. In *Proceedings of the 32nd ACM International Conference on Multimedia*. Association for Computing Machinery, New York, NY, USA, 9116–9125. doi:10.1145/3664647.3681127
- [38] Chien Yao Wang, Alexey Bochkovskiy, and Hong Yuan Mark Liao. 2023. YOLOv7: Trainable Bag-of-Freebies Sets New State-of-the-Art for Real-Time Object Detectors. In *CVPR*. 7464–7475. doi:10.1109/CVPR52729.2023.00721
- [39] Ruixing Wang, Qing Zhang, Chi-Wing Fu, Xiaoyong Shen, Wei-Shi Zheng, and Jiaya Jia. 2019. Underexposed Photo Enhancement Using Deep Illumination Estimation. In *CVPR*. 6842–6850.
- [40] Tao Wang, Kaihao Zhang, Tianrun Shen, Wenhan Luo, Bjorn Stenger, and Tong Lu. 2023. Ultra-High-Definition Low-Light Image Enhancement: A Benchmark and Transformer-Based Method. In *AAAI*, Vol. 37. 2654–2662.
- [41] Wenjing Wang, Huan Yang, Jianlong Fu, and Jiaying Liu. 2024. Zero-Reference Low-Light Enhancement via Physical Quadruple Priors. In *Proceedings of the IEEE/CVF Conference on Computer Vision and Pattern Recognition (CVPR)*. 26057–26066.
- [42] Yang Wang, Yang Cao, Zheng-Jun Zha, Jing Zhang, Zhiwei Xiong, and Wei Zhang. 2019. Progressive Retinex: Mutually Reinforced Illumination-Noise Perception Network for Low-Light Image Enhancement. In *ACM MM*. 2015–2023.
- [43] Yufei Wang, Renjie Wan, Wenhan Yang, Haoliang Li, Lap-Pui Chau, and Alex Kot. 2022. Low-Light Image Enhancement with Normalizing Flow. In *AAAI*. 2604–2612.
- [44] Yufei Wang, Yi Yu, Wenhan Yang, Lanqing Guo, Lap-Pui Chau, Alex C. Kot, and Bihan Wen. 2023. ExposureDiffusion: Learning to Expose for Low-light Image Enhancement. In *ICCV*. 12438–12448.

- [45] Zhendong Wang, Xiaodong Cun, Jianmin Bao, Wengang Zhou, Jianzhuang Liu, and Houqiang Li. 2022. Uformer: A General U-Shaped Transformer for Image Restoration. In *CVPR*. 17662–17672. doi:10.1109/CVPR52688.2022.01716
- [46] Chen Wei, Wenjing Wang, Wenhan Yang, and Jiaying Liu. 2018. Deep Retinex Decomposition for Low-Light Enhancement. In *BMVC*.
- [47] Wenhui Wu, Jian Weng, Pingping Zhang, Xu Wang, Wenhan Yang, and Jianmin Jiang. 2025. Interpretable Optimization-Inspired Unfolding Network for Low-Light Image Enhancement. *IEEE Transactions on Pattern Analysis and Machine Intelligence* 47, 4 (2025), 2545–2562.
- [48] Han Xu, Hao Zhang, Xunpeng Yi, and Jiayi Ma. 2024. CRetinex: A Progressive Color-Shift Aware Retinex Model for Low-Light Image Enhancement. *Int. J. Comput. Vis* (2024), 1–23.
- [49] Ke Xu, Xin Yang, Baocai Yin, and Rynson W.H. Lau. 2020. Learning to Restore Low-Light Images via Decomposition-and-Enhancement. In *CVPR*. 2278–2287. doi:10.1109/CVPR42600.2020.00235
- [50] Xiaogang Xu, Ruixing Wang, Chi-Wing Fu, and Jiaya Jia. 2022. SNR-Aware Low-light Image Enhancement. In *CVPR*. 17693–17703. doi:10.1109/CVPR52688.2022.01719
- [51] Xiaogang Xu, Ruixing Wang, and Jiangbo Lu. 2023. Low-Light Image Enhancement via Structure Modeling and Guidance. In *CVPR*. 9893–9903.
- [52] Canqian Yang, Meiguang Jin, Xu Jia, Yi Xu, and Ying Chen. 2022. AdaInt: Learning Adaptive Intervals for 3D Lookup Tables on Real-Time Image Enhancement. In *CVPR*. IEEE, New Orleans, LA, USA, 17501–17510. doi:10.1109/CVPR52688.2022.01700
- [53] Wenhan Yang, Shiqi Wang, Yuming Fang, Yue Wang, and Jiaying Liu. 2021. Band Representation-Based Semi-Supervised Low-Light Image Enhancement: Bridging the Gap Between Signal Fidelity and Perceptual Quality. *IEEE Trans. Image Process.* 30 (2021), 3461–3473. doi:10.1109/TIP.2021.3062184
- [54] Wenhan Yang, Wenjing Wang, Haofeng Huang, Shiqi Wang, and Jiaying Liu. 2021. Sparse Gradient Regularized Deep Retinex Network for Robust Low-Light Image Enhancement. *IEEE Trans. Image Process.* 30 (2021), 2072–2086. doi:10.1109/TIP.2021.3050850
- [55] Wenhan Yang, Wenjing Wang, Haofeng Huang, Shiqi Wang, and Jiaying Liu. 2021. Sparse Gradient Regularized Deep Retinex Network for Robust Low-Light Image Enhancement. *IEEE Trans. Image Process.* 30 (2021), 2072–2086. doi:10.1109/TIP.2021.3050850
- [56] Xunpeng Yi, Han Xu, Hao Zhang, Linfeng Tang, and Jiayi Ma. 2023. Diff-Retinex: Rethinking Low-light Image Enhancement with A Generative Diffusion Model. In *ICCV*. 12302–12311.
- [57] Syed Waqas Zamir, Aditya Arora, Salman Khan, Munawar Hayat, Fahad Shahbaz Khan, and Ming-Hsuan Yang. 2022. Restormer: Efficient Transformer for High-Resolution Image Restoration. In *CVPR*. 5718–5729. doi:10.1109/CVPR52688.2022.00564
- [58] Syed Waqas Zamir, Aditya Arora, Salman Khan, Munawar Hayat, Fahad Shahbaz Khan, Ming-Hsuan Yang, and Ling Shao. 2020. Learning Enriched Features for Real Image Restoration and Enhancement. In *ECCV*. 492–511.
- [59] Tongshun Zhang, Pingping Liu, Ming Zhao, and Haotian Lv. 2024. DMFourLLIE: Dual-Stage and Multi-Branch Fourier Network for Low-Light Image Enhancement. In *Proceedings of the 32nd ACM International Conference on Multimedia (Melbourne VIC, Australia) (MM '24)*. Association for Computing Machinery, New York, NY, USA, 7434–7443. doi:10.1145/3664647.3681083
- [60] Yonghua Zhang, Xiaojie Guo, Jiayi Ma, Wei Liu, and Jiawan Zhang. 2021. Beyond Brightening Low-light Images. *Int. J. Comput. Vis* 129, 4 (2021), 1013–1037. doi:10.1007/s11263-020-01407-x
- [61] Yonghua Zhang, Jiawan Zhang, and Xiaojie Guo. 2019. Kindling the Darkness: A Practical Low-light Image Enhancer. In *ACM MM*. 1632–1640. doi:10.1145/3343031.3350926
- [62] Zhao Zhang, Huan Zheng, Richang Hong, Mingliang Xu, Shuicheng Yan, and Meng Wang. 2022. Deep Color Consistent Network for Low-Light Image Enhancement. In *CVPR*. 1899–1908.
- [63] Minfeng Zhu, Pingbo Pan, Wei Chen, and Yi Yang. 2020. EEMEFN: Low-Light Image Enhancement via Edge-Enhanced Multi-Exposure Fusion Network. In *AAAI*. 13106–13113.

This supplementary material presents extended technical implementations and experimental evaluations of the proposed IRetinex framework. Section A provides supplementary explanations of key concepts. Section B conducts a computational complexity analysis of the MRES algorithm, establishing its superior efficiency over conventional global MSA methods. A comprehensive qualitative assessment across three benchmark datasets—LOL-v1, LOL-v2-real, and LOL-v2-syn—is provided in Section C to demonstrate the method’s enhancement capabilities. Furthermore, Section D specifically validates its robustness under extreme low-light conditions. Section E systematically examines IRetinex’s applicability in low-light object detection scenarios, revealing its practical advantages. Sections F and G investigate two critical aspects: the efficacy of ICR elimination and its subsequent impact on visual quality improvement. The document concludes with an insightful discussion in Section H, discussing current limitations and outlining promising directions for future research.

A Supplementary explanations

How ICR affects previous methods. ICR induces component entanglement that degrades enhancement quality. As demonstrated on challenging samples (LOL-v2, r0809811bt.png), our method maintains superior component independence and high PSNR, while prior approaches exhibit severe ICR effects—manifested as low cosine similarity—leading to suboptimal performance.

Table 4: Quantitative analysis of ICR effects in Retinex-Based methods. Cosine similarity quantifies feature similarity between illumination and reflectance components.

Metric	KinD	URetinex++	Ours
Cosine Similarity	0.9547	0.9581	0.8996
PSNR (dB)	17.06	16.77	30.35

ICR effects under varying lighting conditions We adjusted lighting intensities utilizing gamma correction on the LOL-v2-synthetic dataset, obtaining bright ($\gamma=0.7$), moderate ($\gamma=1.2$), and dark ($\gamma=1.5$) variants of the dataset. Subsequently, we retrained IRetinex on LOL-v2-syn under varying lighting conditions. Table 5 demonstrates that ablating ICR correction from decomposition and enhancement stages substantially degrades performance, most severely in dark datasets. This confirms that ICR issues critically undermine LLIE efficacy in extreme low-light conditions. Conversely, with ICR correction added, our method exhibited minimal performance fluctuations across all three datasets, confirming that ICR correction enables the model to maintain robustness under varying lighting conditions.

Table 5: Quantitative evaluation of ICR correction under varying illumination levels on LOL-v2-syn.

Setting	Metrics	Bright ($\gamma = 0.7$)	Moderate ($\gamma = 1.2$)	Dark ($\gamma = 1.5$)	Original ($\gamma = 1.0$)
w/o ICR correction	PSNR	19.64	17.02	15.32	17.32
w/o ICR correction	SSIM	0.8098	0.7614	0.4637	0.7963
w/ ICR correction	PSNR	26.96	26.85	26.25	26.84
w/ ICR correction	SSIM	0.9513	0.9512	0.9486	0.9513

The function of feature similarity. In the enhancement stage, the feature similarity is utilized to further enhance the decomposition between illumination and reflectance features. During the

decomposition stage, although ICRR reduces feature similarity between illumination and reflectance features, their cosine similarity remains high (0.7009, Figure 4), proving that reflectance and illumination are not fully decomposed. Therefore, in the enhancement stage, we further leverage feature similarity to first identify the ICR and subsequently transfer it to the corresponding target components for better decomposition.

The function of cosine similarity. We are the first to explore the ICR issue. Therefore, we specifically utilize cosine similarity to assess the mutual independence between illumination and reflectance features. We employ this metric because in high-dimensional feature spaces, cosine similarity is widely adopted for feature similarity measurement (D3still CVPR’24, RIM CVPR’24). Furthermore, we also utilized Pearson correlation to reevaluating the mutual independence and observe similar effect of cosine similarity that the similarity is low (0.8423 vs. 0.6887).

The reason for utilizing the dual color space prior. The illumination priors of RGB and HSV complement each other. Specifically: (1) RGB color space is widely utilized for illumination estimation [18], preserves spectral details but is sensitive to color; (2) HSV color space is inherently resistant to color interference and has the ability to separate illumination (V) from color (H/S) but loses spectral details [3]; (3) Therefore, by combining dual color space priors, the illumination estimation process avoids color impact and preserves spectral details, producing relatively pure illumination and thereby reducing decomposition ICR. We also substituted HSV with YCbCr; however, the linear dependence of Y on RGB limits complementary information integration, resulting in a 0.9 dB PSNR reduction on the LOL-v1 dataset.

The reason for utilizing multi-scale architecture. Our multi-scale architecture is a 5-layer U-shaped network with RCM as its basic unit. Multi-scale architectures are widely utilized in LLIE due to their ability to simultaneously capture global illumination and texture details (KinD [61], URetinex [47]). This ability facilitates ICR identification, thereby driving each component toward its ideal outcome. Ground truth downsampling causes irreversible detail loss (e.g., textures), limiting the model’s ability to reconstruct detail features. To address this, we upsample each scaled feature map to high resolution for loss computation, thereby recovering multi-scale details layer by layer.

Design motivation of ICRR and MRES. ICRR (0.0048M) and MRES (0.101M) are designed to suppress ICR generation and propagation, respectively.

- **ICRR:** During decomposition, ICRR employs dual color space to initialize illumination. Specifically, HSV’s V channel aids RGB color space separates illumination from color to reduce initial ICR (evidenced by low cosine similarity in Fig. 4, this metric measures component similarity, avoiding learned attention bias).

- **MRES:** HSV lacks learning capability, thus unable to adaptively detect ICR for component purification. During enhancement, we design MRES (0.101M), which utilizes feature similarity to identify ICR and drives components toward ideal outcomes.

Differences from cross-attention. Our approach differs from cross-attention in two key aspects:

- **Different goal:** The cross-attention in previous methods (e.g., KinD and Uretinex) focused on illumination-assisted reflectance enhancement without explicit component purification. We are the first

to explore the inter-component residuals (ICR) problem through mutual correction manner, particularly emphasizing illumination-reflectance mutual purification.

- *Different technique*: Different from Uretinex and Retinexformer that directly concatenate/add illumination features in their cross-attention, we employ similarity matrices to identify ICR and supplement them into corresponding component to approach ideal outcomes. Thus, our method and cross-attention are two distinct LLIE solutions.

Rationale for assumptions. Our assumptions are consistent with prior work (KinD [61]). Moreover, Gaussian and Poisson noise are widely utilized to simulate images captured in real-world low-light scenes [18].

B Complexity analysis of ICR estimation

The computational complexity of our ICR estimate primarily stems from the matrix multiplications in Eqs. (14) and (15), i.e., $\mathbb{R}^{C \times HWs^2} \times \mathbb{R}^{HWs^2 \times C}$ and $\mathbb{R}^{HW \times C} \times \mathbb{R}^{C \times C}$. Thus, the complexity $\mathcal{O}(\text{MRES})$ can be expressed as:

$$\begin{aligned} \mathcal{O}(\text{MRES}) &= \mathcal{O}(\text{MRES}_r) + \mathcal{O}(\text{MRES}_l) \\ &= 2 \left[C \cdot (C \cdot HWs^2) + HW \cdot (C \cdot C) \right] \\ &= 2(HWs^2C^2 + HWC^2) \\ &= 2(s^2 + 1)HWC^2, \end{aligned} \quad (20)$$

while the complexity of the global MSA (G-MSA) utilized by previous CNN-Transformer methods SNR-Net [50] is:

$$\mathcal{O}(\text{G-MSA}) = 2(HW)^2C. \quad (21)$$

Comparing Eq. (20) and Eq. (21), we note that $\mathcal{O}(\text{G-MSA})$ is quadratic with input space size (HW), imposing a substantial computational burden. Conversely, $\mathcal{O}(\text{MRES})$ is linear with space size. While we introduce upsampling factor s , the additional cost is lower than HW . For example, in the case where the input image dimension is $256 \times 256 \times 3$, the G-MSA parameter is 2.099M, while MRES requires only 0.101M. Moreover, during inference, as demonstrated in Table 6, IRetinex achieves SOTA performance while utilizing only 5.37M parameters. Processing a 385×385 low-light image with our proposed IRetinex requires merely 0.075 seconds. This represents a 40.87% reduction in inference time compared to SNR-Net (0.127 seconds), balancing efficiency and performance.

Table 6: Inference efficiency comparison on an A800 GPU.

Metric	MIRNet [58]	SNR-Net [50]	Lighten Diffusion [12]	LIEDNet [22]	Ours
PSNR	23.41	24.13	19.94	26.00	26.84
Model Size (M)	31.79	39.12	27.83	4.76	5.37
Inference time (s)	0.263	0.127	0.537	0.084	0.075

C More qualitative results

Figs. 13-15 present qualitative comparisons between our IRetinex and SOTA methods on LOL-v1, LOL-v2-real, and LOL-v2-syn datasets. The enhanced images are evaluated based on three criteria: background noise, structural clarity, and color fidelity.

Fig. 13 presents a comparative analysis of texture restoration results across various methods. Under low-light conditions, wallpaper and drawing paper textures are significantly degraded. Previous

approaches exhibit diverse limitations: RUAS and SGM produce images with insufficient saturation, while EnGAN, RetinexNet, and Uformer amplify background noise. Although DeVigNet, URetinex, and Bread effectively mitigate noise, they introduce over-smoothing artifacts, resulting in loss of fine textures. DeVigNet additionally suffers from structural blurring. In contrast, our proposed method effectively recovers authentic details without introducing additional noise, artifacts, and color distortions, preserving both structural integrity and color authenticity.

Fig. 14 demonstrates the efficacy of various methods in recovering object structures from low-light images. For the underexposed archery target, competing methods exhibit different types of limitations e.g., excessive noise (RUAS, RetinexNet, SCI), structural ambiguity (DeVigNet, MIRNet, Uformer), and color distortion (Zero-DCE, DRBN, EnGAN). In contrast, our IRetinex restores the archery target with minimal noise, accurate color representation and finer texture details. The right image presents a more complex scenario with simultaneous overexposed and underexposed regions. Competing methods struggle with color distortion (RetinexNet, SNR-Net) and accurate lamp structure reconstruction (DeVigNet, MIRNet, Bread). Our IRetinex method effectively handles varying exposure levels, producing reliable enhanced image.

Fig. 15 presents an image with high color saturation, where recovering the vibrant red hues of the petals poses a significant challenge. Some methods struggle to accurately reproduce these saturated colors. For instance, Zero-DCE, DRBN, and LLFormer exhibit various degrees of color distortion, failing to capture the true vibrancy of the petals. In contrast, the enhanced images produced by SNR-Net, SGM, and our IRetinex closely approximate the ground truth. However, while SNR-Net and SGM achieve improved color saturation, they lack the nuanced color transitions within the petals that are characteristic of natural lighting conditions. IRetinex not only achieves accurate color saturation but also exhibits distinct and natural color gradations within the petals. These results demonstrate that our method faithfully emulates the color distribution under normal lighting conditions and better recovers fine-grained color variations, contributing to the visual realism of the enhanced image.

Table 7: Quantitative comparison on SID dataset.

Metrics	Zero-IG	LightenDiffusion	LIEDNet	URetinex++	IRetinex (ours)
PSNR	17.76	16.65	21.66	19.12	25.03
SSIM	0.6483	0.4036	0.6714	0.6022	0.6958

D SID dataset experiments

Beyond standard benchmarks, we evaluated IRetinex on the subset of SID dataset [2], which represent extreme low-light scenarios with near-zero illumination levels—the practical limits of visibility. It contains 2697 RAW short-/long-exposure image pairs captured by Sony $\alpha 7S$ II. We obtained the low-/normal-light RGB images by utilizing the same in-camera signal processing of SID to transfer RAW to RGB. For model evaluation, 2,099 pairs are designated for training and 598 for testing. As quantified in Table 7, IRetinex achieves state-of-the-art performance with PSNR of 25.03 dB and SSIM of 0.6958. It outperforms the second-best LIEDNet by +3.37 dB in PSNR and +0.0244 in SSIM, demonstrating exceptional robustness across diverse lighting environments.

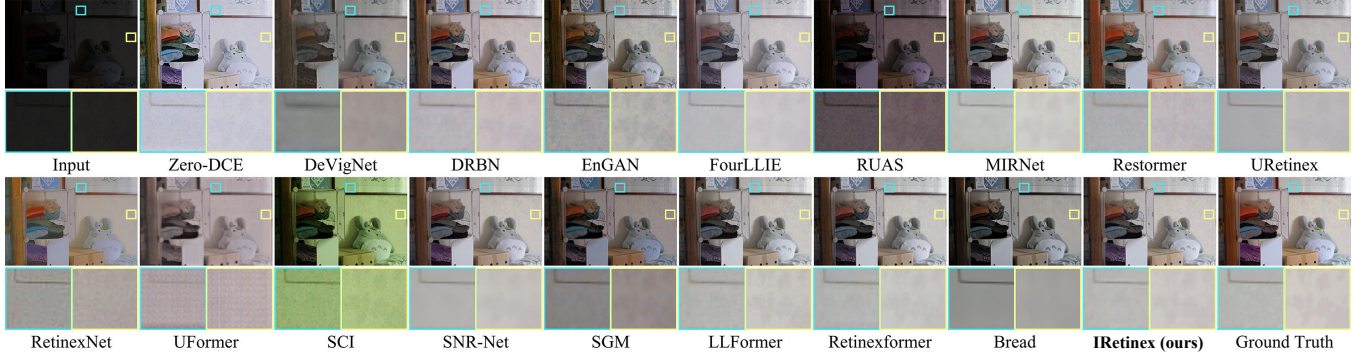


Figure 13: Visual comparison on LOL-v1 dataset. Previous methods collapse by nartifacts, halos, or color distortion. While our algorithm can effectively remove the noise and reconstruct high quality image details.

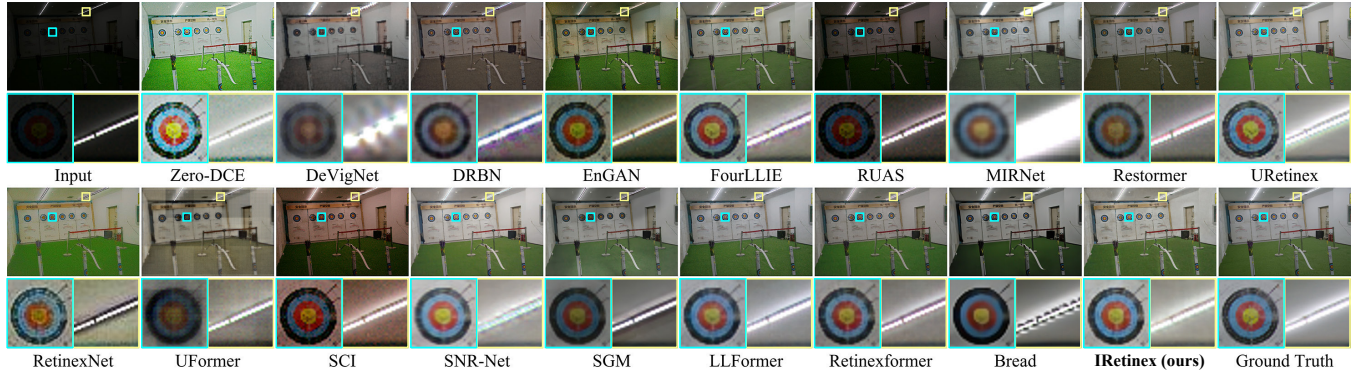


Figure 14: Visual comparison on LOL-v2-real dataset. Previous methods suffer from color and structure distortion. In contrast, our algorithm minimizes noise in underexposed areas, producing reliable enhancement structure.



Figure 15: Visual comparison on LOL-v2-syn dataset. Previous methods struggle to recover the vibrant red of the petals. In contrast, our algorithm exhibits more distinct color gradations, better emulating the natural color distribution under normal light conditions.

E Low-Light object detection

To comprehensively evaluate low-light image enhancement performance, we applied our IRetinex to challenging high-level vision

tasks, *i.e.*, low light object detection. Speciafically, we employed the ExDark dataset [24] to perform multi-object detection on low light images.



Figure 16: Object detection performance in low-light and enhanced images on the ExDark dataset.

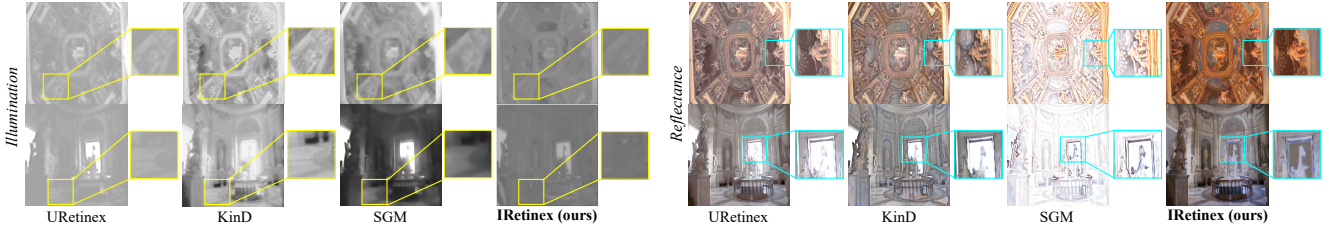


Figure 17: Decomposition results of LLIE methods based on Retinex model on the LOL-v2-syn dataset. All illumination and reflectance components are extracted based on their original implementations.

Table 8: Low-light detection results on ExDark enhanced by different algorithms. The highest result is bolded, while the second highest result is underlined.

Object Categories	Bicycle	Boat	Bottle	Bus	Car	Cat	Chair	Cup	Dog	Motor	People	Table	Mean
DeVigNet [28]	83.6	79.2	81.1	93.7	86.8	72.6	69.1	79.7	80.2	79.8	82.2	64.0	79.3
DMFourLLIE [59]	85.3	81.1	82.8	<u>94.9</u>	87.7	76.6	71.4	<u>81.4</u>	83.1	80.9	<u>83.8</u>	65.3	81.2
UHDFormer [35]	83.5	78.9	81.8	93.4	86.1	74.5	70.8	79.7	80.2	81.6	82.0	65.9	79.9
QuadPrior [41]	84.9	80.2	82.1	94.6	<u>87.8</u>	73.9	71.2	80.9	82.8	80.1	83.5	64.7	80.6
Zero-IG [34]	83.9	79.5	<u>82.9</u>	94.8	<u>87.2</u>	75.8	70.8	80.4	82.3	79.8	82.1	63.9	80.3
LightenDiffusion [12]	83.7	80.5	82.7	93.8	86.3	74.2	71.8	80.4	81.5	<u>81.3</u>	83.4	64.6	80.4
LIEDNet [22]	85.4	80.8	82.3	93.1	86.5	74.9	<u>72.2</u>	80.8	81.1	80.9	83.2	64.3	80.5
URetinex++ [47]	85.3	80.9	82.4	93.6	87.5	75.5	71.5	81.1	82.5	80.8	83.6	65.5	80.9
Retinexformer [1]	<u>86.0</u>	<u>81.3</u>	81.7	94.3	87.5	77.3	72.4	82.4	80.8	80.0	84.5	64.7	81.1
IRetinex (ours)	86.2	81.4	83.5	95.1	88.0	76.7	71.7	81.3	<u>82.9</u>	80.1	83.8	64.8	81.3

E.1 Experimental setup

The ExDark dataset consists of 12 categories and contains 7,363 underexposed images, with 5,896 images utilized for training and 1,467 for testing. Various low-light enhancement methods are employed as pre-processing modules, and the YOLO-v7 [38] detector is trained from scratch for object detection, utilizing average precision (AP) as the evaluation metric.

E.2 Qualitative results

Fig. 12 presents a visual comparison of object detection results in low-light scenes and their enhanced results utilizing competing methods. The fifth row highlights issues with bounding box accuracy, where methods like LightenDiffusion, and URetinex++ fail to fully encompass the cat's tail. The second and sixth row showcases misclassification, with a crumpled paper erroneously

identified as a cat by DeVigNet, Zero-IG, and Retinexformer. In the remaining rows, the comparative methods exhibit varying degrees of accuracy degradation relative to IRetinex, highlighting the persistent challenges in low-light image enhancement for downstream visual tasks. In contrast, images enhanced by IRetinex enable the detector to rectify detection errors and accurately predict bounding boxes across all scenarios. This suggests that our method improves high-level visual understanding, enhancing both classification accuracy and semantic information extraction in challenging low-light conditions.

E.3 Quantitative results

Tab. 8 presents the average precision (AP) for 12 categories as well as the mean AP across all categories. Our IRetinex achieved the highest mean score of 81.3 AP, surpassing the second best method DMFourLLIE by 0.1 AP and the recent fully supervised method Retinexformer by 0.2 AP [1]. Additionally, IRetinex achieved the best results in five object categories: bicycle (86.2 AP), boat (81.4 AP), bottle (83.5 AP), bus (95.1 AP), and car (88.0 AP). Moreover, it closely approaches SOTA values in the remaining seven categories. These quantitative results demonstrate that IRetinex effectively enhances the visual quality of low-light images, ensuring the authenticity of reconstructed details and the accuracy of object information.

F Effectiveness of ICR mitigation

In an ideal ICR-free state, areas of identical materials within the illumination component should display uniform illumination distribution. Simultaneously, the reflectance component should be free from light and shadow effects, accurately representing physical properties of the scene. To validate the ability of our method in removing ICR from different components, we compared the illumination and reflectance components with those obtained from other Retinex-based LLIE models, shown in Fig. 17.

As illustrated in the left portion, the illumination components generated by RetinexNet, URetinex, Kind, and SGM still contain textures in regions of the same material. This indicates that physical properties (partial reflectance) are retained in the illumination component, which decreases the quality of the illumination component. In contrast, our method demonstrates fewer textural residuals and faithfully exhibits the lighting distribution of the scene.

The right figure further demonstrates the effective reduction of ICR in the reflectance components. Specifically, in the comparison methods, the reflectance components still exhibit light and shadows. The physical details of some reflectance images are disrupted by these residuals. The reflectance components also suffer from color distortion and blurred structures. In comparison, IRetinex effectively separates the illumination components, with the reflectance components faithfully representing the physical information of the scene.

G Benefits of ICR mitigation

A well-enhanced low-light image should exhibit similar color and structure distributions to those of a normal-light image. Therefore, to investigate the benefits of ICR removal for image visual quality, we further compare the color and structure distributions with

above methods. The RGB histograms and structural error maps are illustrated in Fig. 19 and Fig. 20, respectively.

As shown in Fig. 19, low-light images exhibit a marked bias in RGB histograms, with pixel values clustered within a low dynamic range. While some methods, *e.g.*, URetinex, partially address this bias, they still display significant pixel value discrepancies. In contrast, IRetinex closely aligns with the ground truth in both visual appearance and RGB histograms, effectively correcting color bias and producing accurate low-light images. Fig. 20 reveals the loss of structure and texture under low-light conditions. Although the compared methods restore some details, they still suffer from structural blurring. For instance, the image produced by SGM still contains artifacts on the lake surface. In contrast, IRetinex effectively corrects the artifacts and shows minimal structural error. These results demonstrate that mitigating the inherent inter-component residuals correct both color and structural deviations, promoting the enhanced images align with normal-light images both visually and in fine details.

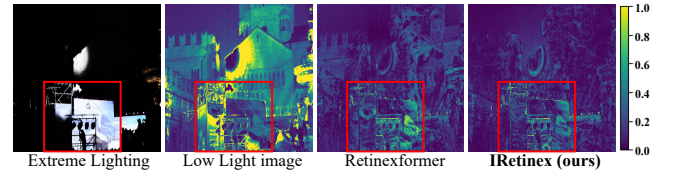


Figure 18: The visualization of the structural error maps. It is challenging to simultaneously recover structural information in both underexposed and overexposed regions.

H Discussion and Limitation

Despite IRetinex demonstrating solid performance in both quantitative and qualitative evaluations, it also faces challenges, particularly in handling extreme over-exposure conditions. For instance, when confronting scenes involving extensive overexposure and extremely low illumination (as illustrated in Fig. 18), both overexposure and underexposure destroy the original image information. Given the complexity of processing such large illumination differences, our method exhibits notable structural error in overexposed regions. To provide a comparative perspective, we present results obtained from Retinexformer [1] and our methods. Evidently, this limitation is not unique to our method but is inherent to all existing approaches in the LLIE field, representing a shared challenge that requires careful consideration. This challenge stems from the inherent complexity of processing extreme lighting in dynamic scenes and remains an active area of research within the LLIE field. In the future, we will explore the removal of inter-component residuals under extreme lighting conditions.

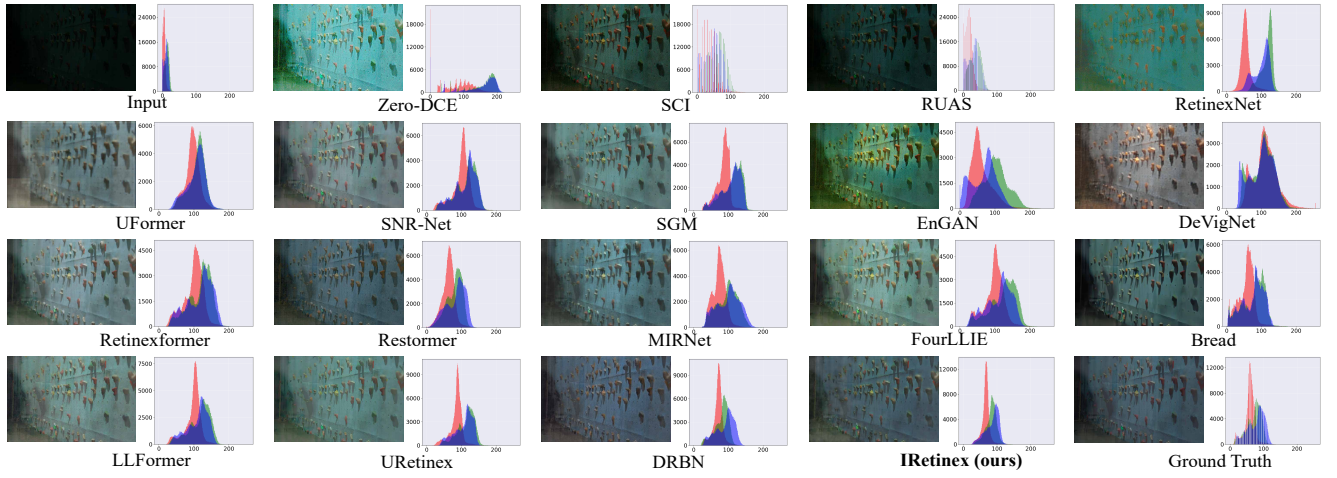


Figure 19: RGB histogram comparison of IRetinex and other LLIE methods on the LOL-v2-real dataset. Red, green, and blue represent R, G, and B color distributions respectively. The x-axis denotes pixel values [0-255], while the y-axis indicates pixel count.

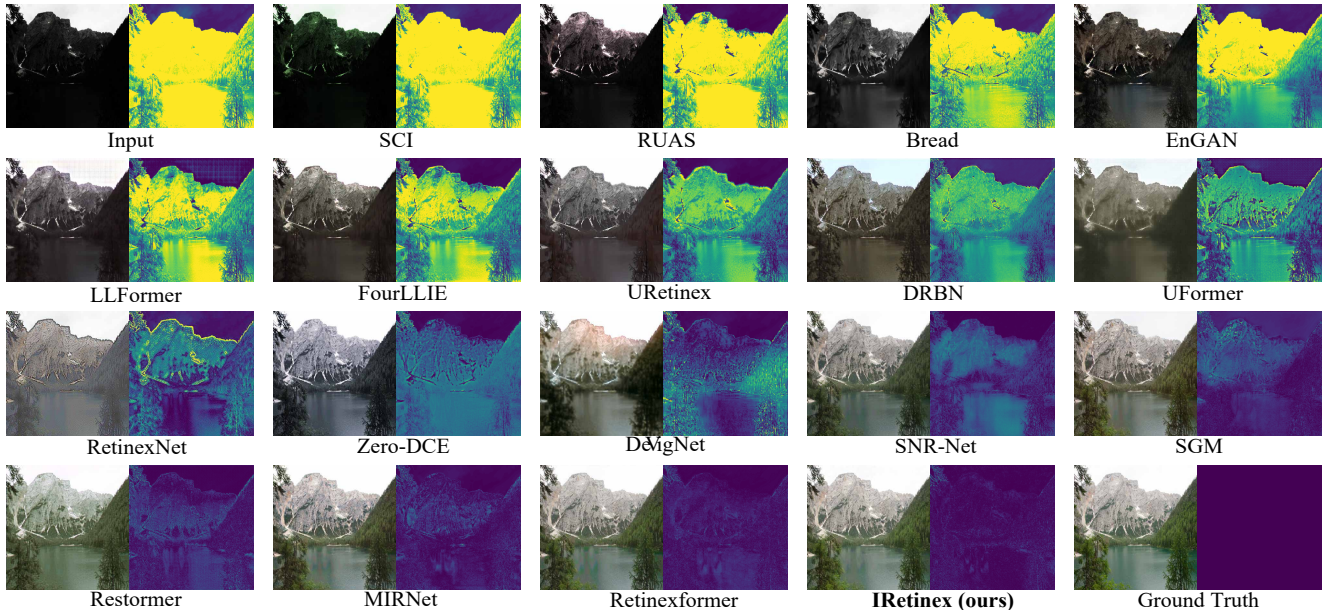


Figure 20: Texture error map comparison between IRetinex and other LLIE methods on the LOL-v2-syn dataset. Color proximity to yellow indicates larger discrepancies, while proximity to blue denotes smaller differences.